

Electric Dipole Spin Resonance of 2D Semiconductor Spin Qubits

Matthew Brooks* and Guido Burkard

Department of Physics, University of Konstanz, D-78464 Konstanz, Germany

Monolayer transition metal dichalcogenides (TMDs) offer a novel two-dimensional platform for semiconductor devices. One such application, whereby the added low dimensional crystal physics (i.e. optical spin selection rules) may prove TMDs a competitive candidate, are quantum dots as qubits. The band structure of TMD monolayers offers a number of different degrees of freedom and combinations thereof as potential qubit bases, primarily electron spin, valley isospin and the combination of the two due to the strong spin orbit coupling known as a Kramers qubit. Pure spin qubits in monolayer MoX_2 (where $X = \text{S}$ or Se) can be achieved by energetically isolating a single valley and tuning to a spin degenerate regime within that valley by a combination of a sufficiently small quantum dot radius and large perpendicular magnetic field. Within such a TMD spin qubit, we theoretically analyse single qubit rotations induced by electric dipole spin resonance. We employ a rotating wave approximation within a second order time dependent Schrieffer-Wolf effective Hamiltonian to derive analytic expressions for the Rabi frequency of single qubit oscillations, and optimise the mechanism or the parameters to show oscillations up to 250 MHz.

I. INTRODUCTION

Transition metal dichalcogenides (TMDs) are graphite-like indirect band-gap semiconductors in bulk, that when isolated down to the monolayer (ML) limit become two-dimensional visible range direct band-gap semiconductors, with a hexagonal crystal lattice structure^{1–5}. The combination of optically addressable electron spin and valley isospin degrees of freedom^{6,7} and strong spin-orbit coupling^{8,9} within a mechanically flexible ML^{10,11} which may be stacked with other ML materials as part of the van der Waals (vdW) heterostructure engineering architecture^{12–14}, has allowed for TMDs to be a viable and desirable host for quantum technologies. Quantum dots (QDs)¹⁵, single-photon emitters^{11,16,17}, gate defined nano-wires^{18,19}, topological materials^{20,21}, ML superconductors^{22,23} as well as spin-^{24,25} and valleytronics^{26,27} have all been proposed or demonstrated with TMD MLs.

Chemically, the semiconducting TMD MLs consist of MX_2 where $M = \text{Mo}$ or W and $X = \text{S}$ or Se , where the M atomic layer is sandwiched between two X atomic layers^{1–4}, with broken inversion symmetry^{1,7,28}, and an $M - X$ alternating hexagonal structure in the plane of the ML^{1,3,29}. The M atoms introduce strong spin-orbit coupling^{8,9}, which with the broken inversion symmetry gives rise to spin-split conduction and valence bands^{6,30,31}. Under an out-of-plane magnetic field, the splitting between the spin states in the conduction band is shifted due to both a spin- and valley-Zeeman effect^{32–35} introduced by a significant Berry curvature at the band-edges^{32,36,37}. Additionally, the Berry curvature allows for optically addressable spin-valley states by correctly applied circularly-polarised light^{6,36}.

QDs in TMD monolayers have been demonstrated by a number of different methods. Electrostatic gating¹⁵, strain^{11,16} and lattice defects³⁸ have all been shown to achieve 0-dimensional behaviour in TMD monolayers. Strain and electrostatic gating however exhibit the most promise for QDs for quantum information purposes³⁹,

and a number of different methods of implementing a qubit in a TMD QD have been proposed including spin-valley Kramers qubits⁴⁰, in which one and two qubit gates have been proposed^{40,41}, and pure-spin qubits⁴². Pure-spin qubits, were shown to be achievable by tuning a combination of the QD radius and the out of plane

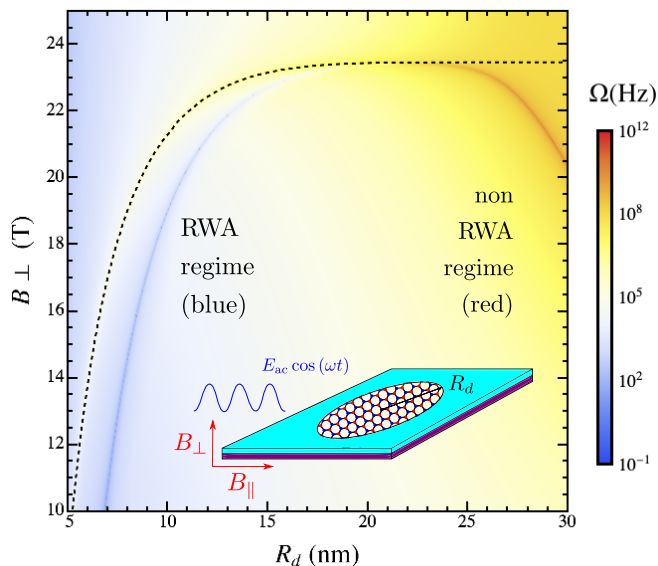


FIG. 1. Rabi frequency Ω of a MoS_2 QD in dependence of the dot radius R_d and out-of-plane magnetic field B_\perp where $E_{ac} = 10^{-2}$ V/nm and $B_\parallel = 1$ T. The black dashed line gives the points of spin degeneracy in the ground states of the K' valley. Note that the region where the RWA is valid is where the frequencies calculated off-resonantly from the spin degeneracy line are small (blue), whilst the region where the maximum Ω deviates from the spin degeneracy line is where the RWA breaks down. Inset: diagram of the setup considered in this work of a gated TMD QD of radius R_d (purple representing the TMD ML and cyan representing the top gate), exposed to a static out-of-plane magnetic field B_\perp , in-plane magnetic field B_\parallel and an in plane AC-electric field E_{ac} .

magnetic field such that, within one valley, a near-spin-degeneracy is reached. The magnetic field required to do so is high ($\sim 20 - 30$ T) when considering only the natural spin- and valley-Zeeman contributions of the ML. However, as previously mentioned, one of the benefits of 2D semiconductors is the access to vdW heterostructure engineering. Thus, it has been shown that by layering TMDs with magnetic monolayers such as CrI₃ and EuS, local time reversal symmetry violation in the TMD occurs, significantly enhancing the valley-Zeeman effect observed in the TMD^{14,43–45}. A similar result may also be achieved with doping⁴⁶. The modularity of vdW heterostructure devices, along with an optically initialisable spin state, makes TMD QDs a strong contender to more conventional bulk semiconductor qubit realisations.

Towards building a 2D quantum processor, the next step, after realising a qubit, is a scheme for single qubit gates, i.e. a reliable method of single-qubit state initialisation and control. In this work, we demonstrate that electric-dipole spin resonance (EDSR) may be achieved in TMD pure-spin qubits. EDSR requires the coupling of the qubit spin states to an external AC-electric field^{47,48}, which drives rotations between the spin states, such that ideally microwave pulses can be used to perform the desired single qubit gate. This has been theoretically shown to be achievable in TMD QDs adopting a Kramers qubit architecture, with the aid of an additional lattice defect to mix the valley states⁴⁰. We show that in a valley-polarised pure-spin qubit architecture, EDSR is achievable and with some parameter optimisation (dot radius, magnetic fields etc.) oscillations of the qubit in the ~ 100 MHz regime are feasible.

This paper is structured as follows, firstly, in Sec. II, the TMD QD Hamiltonian is given and the studied material type and parameter regime for the pure-spin qubit architectures is detailed. Then, in Sec. III, the EDSR mechanism is introduced in detail, giving all relevant matrix elements, as well as an effective qubit Hamiltonian given by a time dependent Schrieffer-Wolff transformation. Thirdly, in Sec. IV, the rotating wave approximation is applied to derive expressions for the Rabi frequency in the rotating frame. This is followed in Sec. V by an analysis of the relevant parameters of the system to maximise the qubit frequency. Lastly, in Sec. VI, a discussion and comparison of this architecture with other known architectures is provided.

II. MONOLAYER TMD QUANTUM DOTS

In this work we assume an electrostatic-gate defined QD in a TMD monolayer. With the appropriate selection of the TMD type, and a sufficiently large external magnetic field, it has been shown that the spin-valley locking may be overcome to provide a host for a valley polarised pure spin qubit⁴².

A. Effective Hamiltonian

The energy levels of a single electron in a TMD quantum dot in a perpendicular magnetic field (B_{\perp}) at the K or K' valleys may be obtained by solving the effective low energy Hamiltonian^{39,42}

$$H_{B_{\perp}}^{\tau,s} = \hbar\omega_c^{\tau,s}\alpha_+\alpha_- + \tau s \frac{\Delta_{\text{cb}}}{2} + \frac{1+\tau}{2} \frac{B_{\perp}}{|B_{\perp}|} \hbar\omega_c^{\tau,s} + \frac{1}{2}(\tau g_{\text{vl}} + s g_{\text{sp}})\mu_B B_{\perp} \quad (1)$$

where $\tau = \pm 1$ is the valley index with $1(-1) \equiv K(K')$, $s = \pm 1$ is the spin index with $1(-1) \equiv \uparrow(\downarrow)$, $\omega_c^{\tau,s}$ is the spin-valley dependent cyclotron frequency, Δ_{cb} is the spin-orbit splitting in the conduction band of the TMD, g_{vl} and g_{sp} are the valley and spin out of plane g-factors respectively and μ_B is the Bohr magneton. The spin-valley dependence of $\omega_c^{\tau,s}$ is due to the spin-valley dependence of the effective mass at the band edges given as $1/m_{\text{eff}}^{\tau,s} = 1/m_{\text{el}}^0 - \tau s/\delta m_{\text{eff}}$ where δm_{eff} is contingent on the TMD type. The modified wavenumber operators α_{\pm} are $\alpha_{\pm} = \mp i l_B q_{\pm}/\sqrt{2}$ where $l_B = \sqrt{\hbar/eB_{\perp}}$ is the magnetic length and $q_{\pm} = q_x \pm i q_y$ where $q_k = -i\partial_k$. The potential of the QD is assumed to be an infinite square well of radius R_d , which is reasonable when assuming the electrostatic gates of the dot to be contacted to or separated by 1-2 layers 2D dielectric hexagonal boron nitride^{15,49}. Thus the quantum dot levels as a function of B_{\perp} and R_d are given as

$$\tilde{\varepsilon}_{n,l}^{\tau,s} = \varepsilon_{n,l}^{\tau,s} + \tau s \frac{\Delta_{\text{cb}}}{2} \quad (2)$$

where

$$\varepsilon_{n,l}^{\tau,s} = \hbar\omega_c^{\tau,s} \left(\frac{1+\tau}{2} \frac{B_{\perp}}{|B_{\perp}|} + \frac{|l|+l}{2} - \gamma_{n,l} \right) + \frac{1}{2}(\tau g_{\text{vl}} + s g_{\text{sp}})\mu_B B_{\perp}. \quad (3)$$

Here $\gamma_{n,l}$ is the n^{th} solution to $M(\gamma_{n,l}, |l|+1, R_d^2/2l_B^2) = 0$, where $M(a, b, c)$ is the confluent hypergeometric function of the first kind, given by the hard-wall boundary condition to Eq. (1).

B. Single dot spin qubit

The spin-valley locking due to spin-orbit coupling and crystal symmetries can be shown to be overcome, resulting in a pure spin qubit⁴² with a TMD QD as opposed to a spin-valley Kramers' qubit⁴⁰. By selecting the appropriate TMD type, dot size and perpendicular magnetic field a regime where $\varepsilon_{n,l}^{K(K'),\uparrow} = \varepsilon_{n,l}^{K(K'),\downarrow}$ may be achieved. MoS₂ is the semiconducting TMD monolayer with the smallest zero field spin splitting in the conduction band

Δ_{cb} and a δm_{eff} such that the condition $\varepsilon_{1,0}^{K',\uparrow} = \varepsilon_{1,0}^{K',\downarrow}$ may be achieved for $B_{\perp} \approx 16$ T in the first excited state ($n = 1, l = -1$) and $B_{\perp} \approx 21$ T in the ground state ($n = 1, l = 0$) assuming $R_d \approx 10$ nm. Assuming that the QD is charged by a valley polarised source, either optically or by valley polarised leads, a pure spin qubit in an MoS₂ monolayer gated quantum dot may be realised.

III. ELECTRIC DIPOLE SPIN RESONANCE

A. External Influences

To achieve control over the qubit spin states, two additional ingredients to the spin-orbit interaction inherent in the crystal are needed; a spin-mixing interaction and a driving field. These are achieved by subjecting the QD to a static in-plane magnetic field and AC in-plane electric field.

The Hamiltonian describing an in-plane magnetic field along the x -direction is given as

$$H_{B_{\parallel}} = \frac{1}{2} \mu_B g_{\parallel} B_{\parallel} s_x \quad (4)$$

where g_{\parallel} is the in-plane g-factor, B_{\parallel} is the in-plane magnetic field and s_i where $i = (x, y, z)$ is the i^{th} spin Pauli matrix, i.e. $s_i = (\hbar/2)\sigma_i$. The in-plane g-factor is assumed in this work to be $g_{\parallel} = 2$, as we assume a clean crystal sample. The out-of-plane g-factor g_s is material

dependent and given by the same 7-band $k \cdot p$ analysis used to derive the effective Hamiltonian Eq. (1)³⁹.

The real-space Hamiltonian of an AC-electric driving field along the x -direction is given as

$$\tilde{H}_{ac} = e x E_{ac} \cos \omega t \quad (5)$$

where e is the elementary charge, E_{ac} and ω denote the field strength and frequency of the AC-field and t is time. In the orbital basis this can be rewritten as approximately (see App. A):

$$H_{ac} = \sigma_x \frac{e E_{ac} R_d \cos(\omega t)}{2\sqrt{2}} \quad (6)$$

where σ_i is the i^{th} orbital Pauli matrix. From these matrix elements, the full Hamiltonian for ESDR in TMD QDs may be written.

B. 4×4 valley-polarised Hamiltonian

Due to our choice of material and B_{\perp} direction (positive along the z -axis), the valley in which the spin qubit is achieved is the K' . From all the elements collected in Sec. II and III A, the full Hamiltonian of the valley-polarised TMD dot with an in-plane magnetic field and AC-electric field is

$$H_{K'} = \frac{1}{2} \begin{pmatrix} 2\varepsilon_{1,0}^{K',\uparrow} - \Delta_{cb} & \mu_B g_{\parallel} B_{\parallel} & \frac{e E_{ac} R_d \cos(\omega t)}{\sqrt{2}} & 0 \\ \mu_B g_{\parallel} B_{\parallel} & 2\varepsilon_{1,0}^{K',\downarrow} + \Delta_{cb} & 0 & \frac{e E_{ac} R_d \cos(\omega t)}{\sqrt{2}} \\ \frac{e E_{ac} R_d \cos(\omega t)}{\sqrt{2}} & 0 & 2\varepsilon_{1,-1}^{K',\uparrow} - \Delta_{cb} & \mu_B g_{\parallel} B_{\parallel} \\ 0 & \frac{e E_{ac} R_d \cos(\omega t)}{\sqrt{2}} & \mu_B g_{\parallel} B_{\parallel} & 2\varepsilon_{1,-1}^{K',\downarrow} + \Delta_{cb} \end{pmatrix} \quad (7)$$

for the qubit basis and the first excited orbital spin states ($\{|l = 0, K', \uparrow\rangle, |l = 0, K', \downarrow\rangle, |l = -1, K', \uparrow\rangle, |l = -1, K', \downarrow\rangle\}$) to which the qubit couples by the driving field. From this, an approximate 2×2 time dependent qubit Hamiltonian may be derived.

C. Time dependent Schrieffer-Wolff transformation

A second order time dependent Schrieffer-Wolff transformation (TDSWT) is employed to isolate a time dependent effective qubit Hamiltonian⁵⁰ (for a complete derivation see App. B). The relevant terms of the transformation are

$$H_{\text{EDSR}}(t) = \tilde{\mathcal{H}}^{(0)} + \tilde{\mathcal{H}}^{(1)} + \tilde{\mathcal{H}}^{(2)}(t) \quad (8)$$

where

$$\tilde{\mathcal{H}}^{(0)} = \sum_{s,l} \varepsilon_{1,l}^{\tilde{r},s} |s, l\rangle \langle s, l| \quad (9a)$$

$$\tilde{\mathcal{H}}^{(1)} = \frac{\mu_B g_{\parallel} B_{\parallel}}{2} s_x \quad (9b)$$

$$\tilde{\mathcal{H}}^{(2)}(t) = \frac{E_{ac}^2 R_d^2 [1 + \cos(2\omega t)]}{36 \hbar \omega_{s,s}^{0,-1}} \sigma_z \quad (9c)$$

where $\omega_{s,s'}^{l,l'}$ is the energy difference between the two QD levels $\varepsilon_{1,l}^{K',s}$ and $\varepsilon_{1,l'}^{K',s'}$ expressed as an angular frequency such that, for example $\varepsilon_{1,0}^{K',\uparrow} - \varepsilon_{1,-1}^{K',\downarrow} = \hbar \omega_{\uparrow,\downarrow}^{0,-1}$. The small

parameters for the TDSWT are the electric field strength $eE_{ac}R_d/\hbar\omega_{\uparrow,\downarrow}^{0,0} \ll 1$ and in plane magnetic field strength $\mu_B g_{\parallel} B_{\parallel}/2\hbar\omega_{\uparrow,\downarrow}^{0,0} \ll 1$. Accordingly, Eq. (8) leads to a block diagonal Hamiltonian for which the relevant time dependent qubit basis portion may be extracted as

$$H_{EDSR}(t) = \begin{pmatrix} \varepsilon_{1,0}^{K',\uparrow} + \frac{e^2 E_{ac}^2 R_d^2 [1 + \cos(2\omega t)]}{16\hbar\omega_{\uparrow,\uparrow}^{0,-1}} & \frac{\mu_B g_{\parallel} B_{\parallel}}{2} \\ \frac{\mu_B g_{\parallel} B_{\parallel}}{2} & \varepsilon_{1,0}^{K',\downarrow} + \frac{e^2 E_{ac}^2 R_d^2 [1 + \cos(2\omega t)]}{16\hbar\omega_{\downarrow,\downarrow}^{0,-1}} \end{pmatrix}. \quad (10)$$

$$\tilde{\Omega} = \frac{3\mu_B g_{\parallel} B_{\parallel} e^2 E_{ac}^2 R_d^2 (\omega_{\downarrow,\downarrow}^{0,-1} - \omega_{\uparrow,\uparrow}^{0,-1})}{4\sqrt{(36\hbar\mu_B g_{\parallel} B_{\parallel} \omega_{\uparrow,\uparrow}^{0,-1} \omega_{\downarrow,\downarrow}^{0,-1})^2 + (e^2 E_{ac}^2 R_d^2 [\omega_{\downarrow,\downarrow}^{0,-1} - \omega_{\uparrow,\uparrow}^{0,-1}] - 36\hbar^2 \omega_{\uparrow,\downarrow}^{0,0} \omega_{\uparrow,\uparrow}^{0,-1} \omega_{\downarrow,\downarrow}^{0,-1})^2}}. \quad (11)$$

Note that in this form, the implicit dependance of the Rabi frequency $\tilde{\Omega}$ on B_{\perp} is within all the $\omega_{s,s'}^{l,l'}(B_{\perp})$ frequencies while the dependance of $\tilde{\Omega}$ on the spin-orbit splitting of the conduction band Δ_{cb} is within $\omega_{\uparrow,\uparrow}^{0,-1}(B_{\perp}, \Delta_{cb})$ and $\omega_{\downarrow,\downarrow}^{0,-1}(B_{\perp}, \Delta_{cb})$. The difference between the two however, present in the numerator of Eq. (11) is not dependent on the spin-orbit splitting. Note that, as the spin splitting due to the spin orbit interaction is decreased, so too is the maximum Rabi frequency achievable, and as $\Delta_{cb} \rightarrow 0$ the in-plane magnetic field small parameter condition of the TDSWT is violated and all of the calculations made up to this point are no longer valid.

A further simplification of Eq. (11) may be given as its dominant term

$$\Omega = \frac{\mu_B g_{\parallel} B_{\parallel} e^2 E_{ac}^2 R_d^2 (\varepsilon_{1,-1}^{K',\uparrow} - \varepsilon_{1,-1}^{K',\downarrow})}{48\Delta_{cb} [\varepsilon_{1,0}^{K',\uparrow} - \varepsilon_{1,-1}^{K',\uparrow}] [\varepsilon_{1,0}^{K',\downarrow} - \varepsilon_{1,-1}^{K',\downarrow}] \hbar^2} \quad (12)$$

assuming $\varepsilon_{1,0}^{K',\uparrow} \approx \varepsilon_{1,0}^{K',\downarrow}$, i.e. operating at the spin qubit regime. The physics of the terms dropped from (11) to give (12) are apparent from the following expansion

$$\tilde{\Omega} = \Omega(1 + \delta_1 + \delta_2 + \dots) \quad (13)$$

where

$$\delta_1 = \frac{e^2 E_{ac}^2 R_d^2 [\omega_{\downarrow,\downarrow}^{0,-1} - \omega_{\uparrow,\uparrow}^{0,-1}]}{36\hbar^2 \omega_{\uparrow,\downarrow}^{0,0} \omega_{\uparrow,\uparrow}^{0,-1} \omega_{\downarrow,\downarrow}^{0,-1}} \quad (14a)$$

$$\times \left(1 + \frac{e^2 E_{ac}^2 R_d^2 [\omega_{\downarrow,\downarrow}^{0,-1} - \omega_{\uparrow,\uparrow}^{0,-1}]}{72\hbar^2 \omega_{\uparrow,\downarrow}^{0,0} \omega_{\uparrow,\uparrow}^{0,-1} \omega_{\downarrow,\downarrow}^{0,-1}} \right)$$

$$\delta_2 = \frac{(\mu_B g_{\parallel} B_{\parallel})^2}{2(\hbar\omega_{\uparrow,\downarrow}^{0,0})^2}. \quad (14b)$$

IV. RABI OSCILLATIONS

From the time-dependent qubit Hamiltonian given in Eq. (10), a transformation into the rotating basis may be performed and the rotating-wave approximation applied to derive the Rabi-oscillation frequency in the rotating frame as

From this, δ_1 can be reasoned as a shift due to the AC stark effect as it is a perturbation in a higher order of E_{ac} and δ_2 is the plane Zeeman shift due to B_{\parallel} . From this form of the Rabi frequency, the effect of the EDSR fields may be probed.

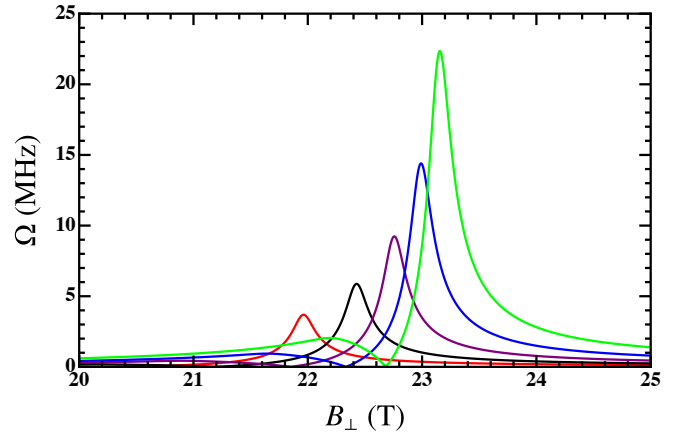


FIG. 2. The out-of-plane magnetic field B_{\perp} dependence of the Rabi frequency Ω for MoS₂ QDs with $R_d = 11$ nm (red), 12 nm (black), 13 nm (purple), 14 nm (blue) and 15 nm (green), with $E_{ac} = 10^{-2}$ V/nm and $B_{\parallel} = 50$ mT.

Firstly, the effect of the strength of the AC-electric field E_{ac} is clearly quadratic. As such, this value shall be fixed at 10^{-2} V/nm, a reasonably achievable electric field amplitude that is consistent with the validity of the small parameter assumption in the following calculations. The effect of B_{\perp} can be seen in both Fig. 2 and 3. Fig. 2 shows the dependance of Ω on B_{\perp} for a number of dot radii. There is a clear peak for each radius and clear minimum, where $\Omega \rightarrow 0$, at which $\omega_{\downarrow,\downarrow}^{0,-1} = \omega_{\uparrow,\uparrow}^{0,-1}$. The reason for this interference is clear in Fig. 3. The avoided crossings for the qubit states and the orbitally excited states do not align with B_{\perp} , as such, there are values

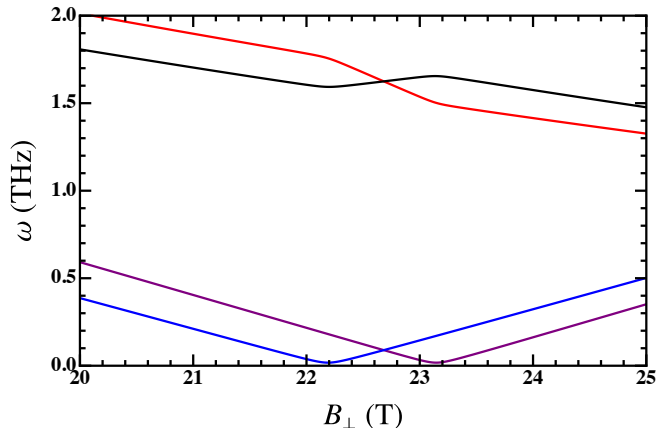


FIG. 3. The out-of-plane magnetic field B_{\perp} dependence of the QD level splittings expressed as angular frequencies $\omega_{\downarrow,\downarrow}^{0,-1}$ (red), $\omega_{\uparrow,\uparrow}^{0,-1}$ (black), $\omega_{\uparrow,\downarrow}^{0,0}$ (purple) and $\omega_{\uparrow,\downarrow}^{-1,-1}$ (blue), for MoS₂ QDs of with $E_{ac} = 10^{-2}$ V/nm, $B_{\parallel} = 50$ mT and $R_d = 15$ nm.

of B_{\perp} that are after one avoided crossing and before the second. This manifests itself in Fig. 3 where each of the kinks in the gradient of the $\omega_{\downarrow,\downarrow}^{0,-1}$ and $\omega_{\uparrow,\uparrow}^{0,-1}$ lines occur at the avoided crossings. It is in between these two kinks that the destructive interference is such that $\omega_{\downarrow,\downarrow}^{0,-1} = \omega_{\uparrow,\uparrow}^{0,-1}$ and $\Omega \rightarrow 0$. The effect of B_{\parallel} is also not fully apparent from Eq. (12). Of course, from the denominator as $B_{\parallel} \rightarrow 0$ so does $\Omega \rightarrow 0$, as there is no spin mixing mechanism at this limit, but the relationship between the two is not linear, as a wider avoided crossing can be detrimental to the rotation speed. As is seen in Fig. 4, there is a clear peak in the achievable Ω at ~ 50 mT, followed by a plateau at ~ 1 T, for a range of radii.

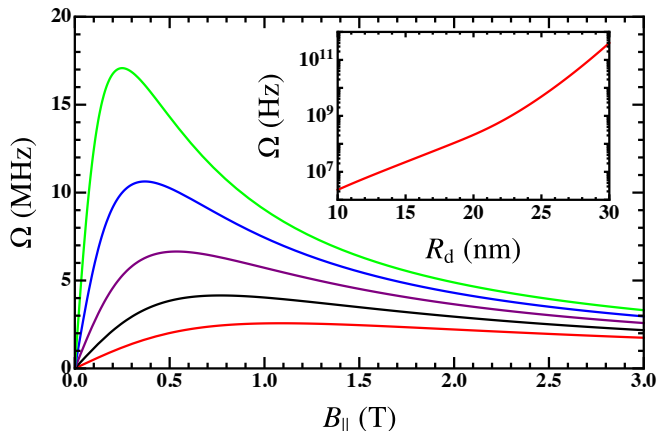


FIG. 4. Rabi frequency on resonance for MoS₂ QDs with $R_d = 11$ nm (red), 12 nm (black), 13 nm (purple), 14 nm (blue) and 15 nm (green), and $E_{ac} = 10^{-2}$ V/nm. Inset: Extracted maximum Rabi frequency Ω with dot radius R_d for MoS₂ QDs with $E_{ac} = 10^{-2}$ V/nm and $B_{\parallel} = 1$ T.

V. OPTIMAL OPERATIONS

Understanding in detail the effects of each of the contributing EDSR mechanisms on the derived single qubit rotational frequency now allows for an optimisation of the EDSR procedure. However, there is still one parameter with which the mechanism may be optimised, the dot radius. Fig. 1 gives $\tilde{\Omega}$ in dependence of R_d and B_{\perp} at constant E_{ac} and B_{\parallel} , showing a clear peak running along the spin-degeneracy line as well as the interference line under the peak. Note that here the full expression $\tilde{\Omega}$ is plotted as to demonstrate where the RWA starts to break down, as for $R_d \gtrsim 22.5$ nm, the higher order terms deviate the peak from around the spin degeneracy point and the Rabi frequency diverges past the reasonable range of the assumed driving frequency (microwave). The reduced form of the Rabi frequency Ω gives exactly the same result below this point, without showing the deviation at larger dot radii. The inset of Fig. 4 shows more explicitly the R_d dependence of the maximum Rabi frequency achievable when at a fixed $B_{\parallel} = 1$ T. Here a near logarithmic increase in achievable Rabi frequency. This trend is easily exploitable but comes with a significant cost in B_{\perp} .

As a proposal for an optimal operational regime, consider a dot of $R_d = 20$ nm. To satisfy both the conditions of the RWA and experimental preferences, only the regime where the qubit detuning is within the microwave range < 300 GHz shall be considered. This is shown in Fig. 5, where a clear peak region at $B_{\perp} = 23.5$ T and $B_{\parallel} = 20$ mT can be seen. At this optimised point a very desirable Rabi frequency of ~ 250 MHz is reached. However, there is a band where Rabi frequencies ~ 100 MHz are attainable, allowing for less precise control of the magnetic fields to access a desirable frequency range.

VI. DISCUSSION

To implement a pure-spin qubit with fast single gate operations we find that a good choice consists of an MoS₂ QD of radius $R_d = 20$ nm, in an external out-of-plane magnetic field $B_{\perp} = 23.5$ T, in-plane magnetic field $B_{\parallel} = 20$ mT and a microwave frequency AC-electric field of strength $E_{ac} = 10^{-2}$ V/nm. This allows for a Rabi frequency of $\Omega = 250$ MHz. All of the assumed field parameters are within reasonable viability. The B_{\perp} requirement is high, however this can be reasonably mitigated by vdW heterostructure engineering with magnetic monolayers. All calculations given assume the qubit is implemented in a free standing TMD ML, to give an upper limit on what would be experimentally required. Recent advances in vdW heterostructure engineering have shown that significant valley-Zeeman enhancement can be achieved by layering the TMD on a ML or low dimensional magnetic material^{14,43,44}. Ideally, a vdW stack of hBN - CrI₃ or EuS - MoS₂ - hBN would be used to implement a TMD spin quantum processor. The purpose

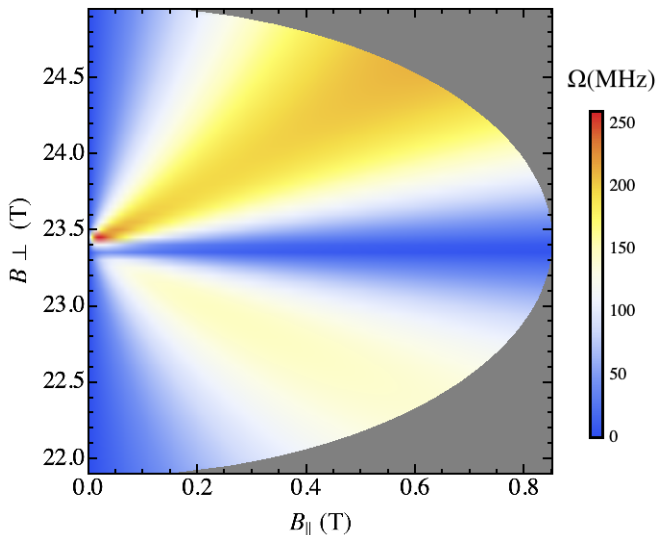


FIG. 5. The out-of-plane B_{\perp} and in-plane B_{\parallel} magnetic field dependencies of the Rabi frequency Ω for an MoS₂ QD of radius $R_d = 20$ nm where $E_{ac} = 10^{-2}$ V/nm only within the microwave qubit detuning range.

of the hBN is to protect the other MLs from degradation as well as improve the optical response of the TMD for state initialisation^{51–53}.

The gate speed shown here is an order of magnitude faster within reasonable experimental limitations than has been shown in the alternative single dot approach to TMD qubits, the Kramers qubit⁴⁰. This assumes a clean crystal, unlike the Kramers qubit that requires a defect to mix the valleys. While defects are currently inherent to TMD samples, they are usually undesirable, and in the proposed pure-spin qubit scheme offer a dephasing mechanism. However, the K -valley levels are higher in energy and become more energetically separated at lower R_d , therefore, some tradeoff between gate speed and stability can be made in the case of valley-mixing crystal defects. Additionally, there has been recent significant progress in synthesising low defect rate monolayers by chemical as opposed to mechanical means⁵⁴.

The ~ 100 MHz single gate rotations makes this 2D qubit implementation competitive with more conventional bulk semiconductor architectures. Both GaAs and Si 2D electron gas gated single spin qubits have experimentally shown Rabi oscillations in the order of ~ 10 MHz^{47,55,56}. However, in TMDs, these fast gate speeds are required as spin lifetimes have only been measured up to a few nanoseconds⁵⁷. This is however, expected to improve with the advent of cleaner crystal samples. The promise of similar to improved speeds attainable with the TMD device proposed here, in a flexible and optically active medium, further positions 2D semiconductors as exciting novel materials for quantum device applications.

VII. ACKNOWLEDGEMENTS

We acknowledge helpful discussions with A. David, F. Ginzler, M. Russ and V. Shkolnikov and funding through both the European Union by way of the Marie Curie ITN Spin-Nano and the DFG through SFB 767.

Appendix A: Dipole Matrix

The dipole matrix elements represent the off-diagonal elements that in the case of this work couple the qubit states with the first excited orbital states. These are calculated as follows

$$d_{nl,n'l'} = \langle \psi_{nl} | \tilde{H}_{ac} | \psi_{n'l'} \rangle \quad (\text{A1})$$

where \tilde{H}_{ac} is given by (5). Here the wavefunctions are derived from Eq. (1) as⁴²

$$\psi_{n,l} = \mathcal{A}(\gamma_{n,l}, \rho) e^{i\theta} \rho^{|l|/2} e^{-\rho/2} M(\gamma_{n,l}, |l| + 1, \rho) \quad (\text{A2})$$

where $\mathcal{A}(\gamma_{n,l}, \rho)$ is the normalising factor. Importantly for this work, the matrix element $\langle \psi_{n,l} | \tilde{H}_{ac} | \psi_{n,l} \rangle = 0$ while $\langle \psi_{n,l} | \tilde{H}_{ac} | \psi_{n,l'} \rangle \neq 0$ for $l \neq l'$. The value of these matrix elements can be calculated numerically. The corresponding matrix element is dependent on B_{\perp} and R_d , however, we find that the dependence on B_{\perp} is so slight ($< 0.01\%$) that for this work we shall simply assume

$$\langle \psi_{0,1} | \tilde{H}_{ac} | \psi_{0,0} \rangle \approx \frac{eE_{ac}R_d}{2\sqrt{2}}. \quad (\text{A3})$$

Appendix B: Full TDSWT Derivation

The time-dependent Schrieffer-Wolff transformation is a perturbative method to derive an effective block diagonal Hamiltonian $\tilde{\mathcal{H}}(t)$ from a dense Hamiltonian $\mathcal{H}(t)$ such as Eq. (7)⁵⁰. We proceed by applying the unitary transformation $U(t) = e^{-S(t)}$, such that

$$\tilde{\psi}(t) = e^{-S(t)} \psi(t), \quad (\text{B1})$$

and, using the time-dependent Schrödinger equation, $-i\hbar \frac{\partial}{\partial t} \psi(t) + \mathcal{H}(t)\psi(t) = 0$, leading to the transformed Hamiltonian

$$\tilde{\mathcal{H}}(t) = e^{-S(t)} \mathcal{H}(t) e^{S(t)} + i\hbar \frac{\partial e^{-S(t)}}{\partial t} e^{S(t)}. \quad (\text{B2})$$

Here $S(t)$ is some block off-diagonal matrix. From this set up, a power-series expansion can then be applied which can be simplified to give

$$\tilde{\mathcal{H}}(t) = \sum_{j=0}^{\infty} \frac{1}{j!} [\mathcal{H}(t), S(t)]^{(j)} - i\hbar \sum_{j=0}^{\infty} \frac{1}{(j+1)!} \left[\dot{S}(t), S(t) \right]^{(j)} \quad (\text{B3})$$

where $[A, B]^{(0)} = A$ and $[A, B]^{(n+1)} = [[A, B]^{(n)}, B]$. Here, $S(t)$ is solved for by assuming $\tilde{\mathcal{H}}(t)_{\text{off-diagonal}} = 0$. At this point no approximation has been made. The approximation made to solve Eq. (B2) such that $\tilde{\mathcal{H}}(t)_{\text{off-diagonal}} = 0$ is a power-series expansion of the small parameters (in plane electric and magnetic fields) of the $S(t)$ matrix

$$S(t) = S(t)^{(1)} + S(t)^{(2)} + S(t)^{(3)} + \dots \quad (\text{B4})$$

where $S(t)_n$ is the n^{th} order of the power-series.

At this point, all the necessary definitions have been made to perform a general TDSWT, as such, now only a second order perturbation of the Eq. (7) will be considered with small parameters are the electric field strength $eE_{\text{ac}}R_d/\hbar\omega_{\uparrow,\downarrow}^{0,0}(B_{\perp}) \ll 1$ and in-plane magnetic field strength $\mu_B g_{\parallel} B_{\parallel}/\hbar\omega_{\uparrow,\downarrow}^{0,0}(B_{\perp}) \ll 1$. The effective Hamiltonian with corrections up to second order is given by

$$\tilde{\mathcal{H}}(t) = \tilde{\mathcal{H}}^{(0)} + \tilde{\mathcal{H}}^{(1)} + \tilde{\mathcal{H}}(t)^{(2)}. \quad (\text{B5})$$

From this, the expansions in $\tilde{\mathcal{H}}(t)$ can be solved from

Eq. (B2) as

$$\tilde{\mathcal{H}}^{(0)} = \mathcal{H}_0 \quad (\text{B6a})$$

$$\tilde{\mathcal{H}}^{(1)} = \mathcal{H}_1 \quad (\text{B6b})$$

$$\tilde{\mathcal{H}}^{(2)}(t) = \frac{1}{2} \left[\mathcal{H}_2(t), S(t)^{(1)} \right]. \quad (\text{B6c})$$

Here \mathcal{H}_0 is the diagonal part of Eq. (B2), \mathcal{H}_1 is the block diagonal part omitting the diagonal part of Eq. (B2) and $\mathcal{H}_2(t)$ is the block off-diagonal part of Eq. (B2), which for the case of the EDSR mechanism described translates as the QD levels $\mathcal{H}_0 = \sum_{s,l} \varepsilon_{1,l}^{K',s} |s, l\rangle \langle s, l|$, in-plane magnetic field Eq. (4) for \mathcal{H}_1 and AC-electric field maxtrix elements Eq. (6) for \mathcal{H}_2 . Only $S_1(t)$ needs to be solved for, which is done by applying the $\tilde{\mathcal{H}}(t)_{\text{off-diagonal}} = 0$ condition giving

$$\left[\mathcal{H}_0, S(t)^{(1)} \right] = -\mathcal{H}_2. \quad (\text{B7})$$

So finally, a block diagonal of the qubit and the excited orbital space may be approximated where the qubit space of Eq. (B5) is given as Eq. (10).

-
- * matthew.brooks@uni-konstanz.de
- ¹ Q. H. Wang, K. Kalantar-Zadeh, A. Kis, J. N. Coleman, and M. S. Strano, *Nat. Nanotechnol.* **7**, 699 (2012).
 - ² A. Kumar and P. Ahluwalia, *Eur. Phys. J. B* **85**, 186 (2012).
 - ³ M. Chhowalla, H. S. Shin, G. Eda, L.-J. Li, K. P. Loh, and H. Zhang, *Nat. Chem.* **5**, 263 (2013).
 - ⁴ Y. Zhang, T.-R. Chang, B. Zhou, Y.-T. Cui, H. Yan, Z. Liu, F. Schmitt, J. Lee, R. Moore, Y. Chen, *et al.*, *Nat. Nanotechnol.* **9**, 111 (2014).
 - ⁵ A. Kormányos, G. Burkard, M. Gmitra, J. Fabian, V. Zólyomi, N. D. Drummond, and V. Falco, *2D Materials* **2**, 022001 (2015).
 - ⁶ D. Xiao, G.-B. Liu, W. Feng, X. Xu, and W. Yao, *Phys. Rev. Letts.* **108**, 196802 (2012).
 - ⁷ X. Xu, W. Yao, D. Xiao, and T. F. Heinz, *Nat. Phys.* **10**, 343 (2014).
 - ⁸ Z. Zhu, Y. Cheng, and U. Schwingenschlögl, *Phys. Rev. B* **84**, 153402 (2011).
 - ⁹ G. Wang, C. Robert, A. Suslu, B. Chen, S. Yang, S. Alamdari, I. C. Gerber, T. Amand, X. Marie, S. Tongay, *et al.*, *Nat. Comms.* **6**, 10110 (2015).
 - ¹⁰ D. Çakır, F. M. Peeters, and C. Sevik, *App. Phys. Lett.* **104**, 203110 (2014).
 - ¹¹ C. Palacios-Berraquero, D. M. Kara, A. R.-P. Montblanch, M. Barbone, P. Latawiec, D. Yoon, A. K. Ott, M. Loncar, A. C. Ferrari, and M. Atatüre, *Nat. Commun.* **8**, 15093 (2017).
 - ¹² A. K. Geim and I. V. Grigorieva, *Nature* **499**, 419 (2013).
 - ¹³ F. Withers, O. Del Pozo-Zamudio, A. Mishchenko, A. Rooney, A. Gholinia, K. Watanabe, T. Taniguchi, S. Haigh, A. Geim, A. Tartakovskii, *et al.*, *Nat. Mater.* **14**, 301 (2015).
 - ¹⁴ D. Zhong, K. L. Seyler, X. Linpeng, R. Cheng, N. Sivadas, B. Huang, E. Schmidgall, T. Taniguchi, K. Watanabe, M. A. McGuire, *et al.*, *Sci. Adv.* **3**, e1603113 (2017).
 - ¹⁵ R. Pisoni, Z. Lei, P. Back, M. Eich, H. Overweg, Y. Lee, K. Watanabe, T. Taniguchi, T. Ihn, and K. Ensslin, *Appl. Phys. Letts.* **112**, 123101 (2018).
 - ¹⁶ A. Branny, S. Kumar, R. Proux, and B. D. Gerardot, *Nat. Commun.* **8**, 15053 (2017).
 - ¹⁷ J. Kern, I. Niehues, P. Tonndorf, R. Schmidt, D. Wigger, R. Schneider, T. Stiehm, S. Michaelis de Vasconcellos, D. E. Reiter, T. Kuhn, *et al.*, *Adv. Mater.* **28**, 7101 (2016).
 - ¹⁸ J. Lin, O. Cretu, W. Zhou, K. Suenaga, D. Prasai, K. I. Bolotin, N. T. Cuong, M. Otani, S. Okada, A. R. Lupini, *et al.*, *Nat. Nanotechnol.* **9**, 436 (2014).
 - ¹⁹ J. Klinovaja and D. Loss, *Phys. Rev. B* **88**, 075404 (2013).
 - ²⁰ Z. Fei, T. Palomaki, S. Wu, W. Zhao, X. Cai, B. Sun, P. Nguyen, J. Finney, X. Xu, and D. H. Cobden, *Nat. Phys.* **13**, 677 (2017).
 - ²¹ Y. Ma, L. Kou, X. Li, Y. Dai, and T. Heine, *Phys. Rev. B* **93**, 035442 (2016).
 - ²² X. Xi, Z. Wang, W. Zhao, J.-H. Park, K. T. Law, H. Berger, L. Forró, J. Shan, and K. F. Mak, *Nat. Phys.* **12**, 139 (2016).
 - ²³ Y.-T. Hsu, A. Vaezi, M. H. Fischer, and E.-A. Kim, *Nat. Comms.* **8**, 14985 (2017).
 - ²⁴ A. F. Morpurgo, *Nat. Phys.* **9**, 532 (2013).
 - ²⁵ T. S. Ghiasi, J. Ingla-Aynés, A. A. Kaverzin, and B. J. van Wees, *Nano Letts.* **17**, 7528 (2017).
 - ²⁶ J. R. Schaibley, H. Yu, G. Clark, P. Rivera, J. S. Ross,

- K. L. Seyler, W. Yao, and X. Xu, *Nat. Rev. Mater.* **1**, 16055 (2016).
- ²⁷ Y. K. Luo, J. Xu, T. Zhu, G. Wu, E. J. McCormick, W. Zhan, M. R. Neupane, and R. K. Kawakami, *Nano Letts.* **17**, 3877 (2017).
- ²⁸ X. Yin, Z. Ye, D. A. Chenet, Y. Ye, K. O'Brien, J. C. Hone, and X. Zhang, *Science* **344**, 488 (2014).
- ²⁹ H. Zeng and X. Cui, *Chem. Soc. Rev.* **44**, 2629 (2015).
- ³⁰ K. Kořmider, J. W. González, and J. Fernández-Rossier, *Phys. Rev. B* **88**, 245436 (2013).
- ³¹ A. Kormányos, V. Zólyomi, N. D. Drummond, P. Rakyta, G. Burkard, and V. I. Fal'ko, *Phys. Rev. B* **88**, 045416 (2013).
- ³² A. Srivastava, M. Sidler, A. V. Allain, D. S. Lembke, A. Kis, and A. Imamoglu, *Nat. Phys.* **11**, 141 (2015).
- ³³ Z. Wang, J. Shan, and K. F. Mak, *Nat. Nanotechnol.* **12**, 144 (2017).
- ³⁴ R.-L. Chu, X. Li, S. Wu, Q. Niu, W. Yao, X. Xu, and C. Zhang, *Phys. Rev. B* **90**, 045427 (2014).
- ³⁵ T. Lyons, S. Dufferwiel, M. Brooks, F. Withers, T. Taniguchi, K. Watanabe, K. Novoselov, G. Burkard, and A. Tartakovskii, *arXiv preprint arXiv:1811.08835* (2018).
- ³⁶ H. Yu, G.-B. Liu, P. Gong, X. Xu, and W. Yao, *Nat. Comms.* **5**, 3876 (2014).
- ³⁷ A. Kormányos, V. Zólyomi, V. I. Fal'ko, and G. Burkard, *Phys. Rev. B* **98**, 035408 (2018).
- ³⁸ M. Brotons-Gisbert, A. Branny, S. Kumar, R. Picard, R. Proux, M. Gray, K. S. Burch, K. Watanabe, T. Taniguchi, and B. D. Gerardot, *arXiv preprint arXiv:1810.02855* (2018).
- ³⁹ A. Kormányos, V. Zólyomi, N. D. Drummond, and G. Burkard, *Phys. Rev. X* **4**, 011034 (2014).
- ⁴⁰ G. Széchenyi, L. Chirulli, and A. Pályi, *2D Materials* **5**, 035004 (2018).
- ⁴¹ A. David, G. Burkard, and A. Kormányos, *2D Materials* **5**, 035031 (2018).
- ⁴² M. Brooks and G. Burkard, *Phys. Rev. B* **95**, 245411 (2017).
- ⁴³ C. Zhao, T. Norden, P. Zhang, P. Zhao, Y. Cheng, F. Sun, J. P. Parry, P. Taheri, J. Wang, Y. Yang, *et al.*, *Nat. Nanotechnol.* **12**, 757 (2017).
- ⁴⁴ K. L. Seyler, D. Zhong, B. Huang, X. Linpeng, N. P. Wilson, T. Taniguchi, K. Watanabe, W. Yao, D. Xiao, M. A. McGuire, *et al.*, *Nano Letts.* **18**, 3823 (2018).
- ⁴⁵ B. Huang, G. Clark, E. Navarro-Moratalla, D. R. Klein, R. Cheng, K. L. Seyler, D. Zhong, E. Schmidgall, M. A. McGuire, D. H. Cobden, *et al.*, *Nature* **546**, 270 (2017).
- ⁴⁶ Z. Wang, K. F. Mak, and J. Shan, *Phys. Rev. Letts.* **120**, 066402 (2018).
- ⁴⁷ M. Russ and G. Burkard, *J. Phys.: Cond. Mat* **29**, 393001 (2017).
- ⁴⁸ V. N. Golovach, M. Borhani, and D. Loss, *Phys. Rev. B* **74**, 165319 (2006).
- ⁴⁹ G.-H. Lee, X. Cui, Y. D. Kim, G. Arefe, X. Zhang, C.-H. Lee, F. Ye, K. Watanabe, T. Taniguchi, P. Kim, *et al.*, *ACS nano* **9**, 7019 (2015).
- ⁵⁰ J. Romhányi, G. Burkard, and A. Pályi, *Phys. Rev. B* **92**, 054422 (2015).
- ⁵¹ Y. Zhou, G. Scuri, D. S. Wild, A. A. High, A. Dibos, L. A. Jauregui, C. Shu, K. De Greve, K. Pistunova, A. Y. Joe, *et al.*, *Nat. Nanotechnol.* **12**, 856 (2017).
- ⁵² F. Cadiz, E. Courtade, C. Robert, G. Wang, Y. Shen, H. Cai, T. Taniguchi, K. Watanabe, H. Carrere, D. Lagarde, *et al.*, *Phys. Rev. X* **7**, 021026 (2017).
- ⁵³ G. Scuri, Y. Zhou, A. A. High, D. S. Wild, C. Shu, K. De Greve, L. A. Jauregui, T. Taniguchi, K. Watanabe, P. Kim, *et al.*, *Phys. Rev. Letts.* **120**, 037402 (2018).
- ⁵⁴ K. Pistunova, L. Jauregui, A. Joe, K. De Greve, A. Sushko, D. Rhodes, J. Hone, H. Park, M. Lukin, and P. Kim, *Bulletin of the American Physical Society* (2019).
- ⁵⁵ S. Nadj-Perge, S. Frolov, E. Bakkers, and L. P. Kouwenhoven, *Nature* **468**, 1084 (2010).
- ⁵⁶ E. Kawakami, P. Scarlino, D. R. Ward, F. Braakman, D. Savage, M. Lagally, M. Friesen, S. N. Coppersmith, M. A. Eriksson, and L. Vandersypen, *Nat. Nanotechnol.* **9**, 666 (2014).
- ⁵⁷ L. Yang, N. A. Sinitsyn, W. Chen, J. Yuan, J. Zhang, J. Lou, and S. A. Crooker, *Nature Physics* **11**, 830 (2015).